

# Interplay between topology and localization on superconducting circuits

Xin Guan<sup>1</sup> and Gang Chen<sup>2,3,4</sup>

<sup>1</sup>*Department of Materials and Chemical Engineering, Taiyuan University, Taiyuan, DC 030032, China\**

<sup>2</sup>*State Key Laboratory of Quantum Optics and Quantum Optics Devices,*

*Institute of Laser Spectroscopy, Shanxi University, Taiyuan, DC 030006, China*

<sup>3</sup>*Collaborative Innovation Center of Extreme Optics, Shanxi University, Taiyuan, DC 030006, China*

<sup>4</sup>*School of Physics, Zhengzhou University, Zhengzhou, DC 450001, China*

Topological insulators lie at the forefront of condensed matter physics. However strong disorder can destroy the topological states and make all states become localized. In this paper, we investigate the competition between topology and localization in the one-dimensional Su-Schrieffer-Heeger (SSH) model with controllable off-diagonal quasi-periodic modulations on superconducting circuits. By utilizing external ac magnetic fluxes, each transmon can be driven and all coupling strengths can be tuned independently. Based on this model we construct phase diagrams that illustrate the extended topologically nontrivial, critical localization, and coexisting topological and critical localization phases. The dynamics of the qubits' excitations are also discussed in this paper, revealing distinct quantum state transfers resulting from the interplay between topology and localization. Furthermore, we propose a method for detecting different quantum phases using current experimental setups.

## I. INTRODUCTION

Recent experimental breakthrough of superconducting circuits has opened up a new avenue for processing quantum computing[1–3] and quantum information[4–6], as well as implementing quantum simulation[7–9]. Due to the superconducting circuits can be fabricated into different lattice structures, a wide range of condensed matter phenomena can be simulated, such as chiral physics and spin clusters[10], topological semimetal[11, 12], quantum walks[2, 13], quantum phase transitions[14, 15], and many-body quench dynamics[8]. A recent experiment has successfully engineered a chain of qubits on superconducting circuits with tunable couplings through external drivings[16]. Utilizing this experimental setup, a meticulous study has successfully observed the topological magnon insulator and detected its winding number[17]. These experiments provide a novel approach for investigating exotic topological properties.

On the other hand, topological insulators (TIs)[18–29] have received considerable attention in the past decades. As is well known, in addition to possessing a bulk gap, topological insulators (TIs) exhibit symmetry-protected gapless states localized at their boundaries. The topological properties of TIs are robust against weak disorders such as fluctuations, imperfections in device fabrications, and environmental noises. Consequently, TIs have found numerous applications in quantum computation and information processing. However, when subjected to strong enough disorder, the topological state can be destroyed and replaced by a localization state. Additionally, moderate levels of disorder can induce a topological Anderson insulator[30–36]. It is intriguing to investigate the interplay between topology and localization. Quasi-periodic disorder and dimer lattice structure have attracted much attention as means to induce localization and topological states, respectively. The famous Aubry-André(AA)[37–42] and Su-Schrieffer-Heeger(SSH)[43–51] models are ab-

stracted, both of which have been realized in superconducting circuits[39, 49]. Therefore to design a qubits chain with staggered coupling strength and controllable off-diagonal quasi-periodic modulations is appealing.

In this paper, we propose a practical approach to realize the one-dimensional SSH model on superconducting circuits with controllable off-diagonal quasi-periodic modulations. Specifically each transmon is driven by an external ac magnetic flux via the flux-bias line. All parameters can be independently adjusted by manipulating the amplitudes and frequencies of the drivings. Through this generalized SSH model, we have discovered extended topologically nontrivial, critical localization, and co-existing topological and critical localization phases transitions. We utilize the winding number and inverse participation ratio (IPR) to characterize the topological and localization properties, respectively. Additionally, we discuss the dynamics of qubit excitations in this paper. We observe different quantum state transfers induced by competition between topology and localization. Finally, we address possible experimental observations of these quantum phases. Herein, we introduce the mean chiral displacement (MCD) as a means to probe the winding number. Our results provide a novel avenue for exploring exotic quantum phases and dynamic behaviors arising from the interplay between dimerization and quasi-periodic disorder strengths on superconducting circuits.

## II. MODEL AND HAMILTONIAN

The method for implementing a one-dimensional SSH model with quasi-periodicity on superconducting circuits is as follow. We consider a chain of transmon qubits that are capacitively coupled to their next-nearest neighbor qubits, as illustrated in Fig. 1(a). The corresponding Lagrangian is written as

$$\mathcal{L} = \sum_j \left[ \frac{C_j}{2} \dot{\phi}_j^2 + E_j^{J0} \cos \left( \frac{\phi_j}{\phi_0} \right) \right] + \sum_{\langle i,j \rangle} \left[ \frac{C_{ij}}{2} (\dot{\phi}_i - \dot{\phi}_j)^2 \right] \quad (1)$$

\*Electronic address: [guanxin810712@163.com](mailto:guanxin810712@163.com)

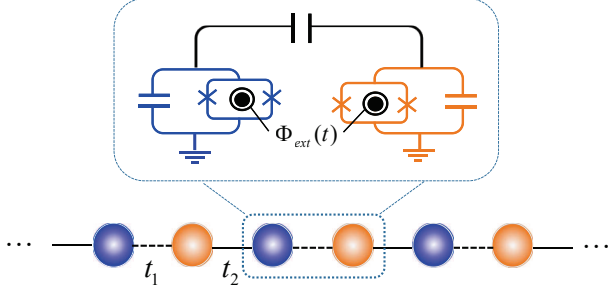


FIG. 1: Schematic diagram of transmon qubits chain with tunable coupling strengths. All transmon qubits are coupled with their nearest-neighbor qubits by capacitors. (a) Illustration of the detail circuits of two coupled qubits. (b) Schematic diagram of the generalized SSH model with  $t_1$  and  $t_2$  as the coupling strengths.  $\Phi_{ext}(t)$  is the external ac magnetic flux.

Here,  $C_j$  and  $E_j^{J0}$  represent the effective capacitance and the Josephson energy of the  $j$ th transmon qubit.  $C_{ij}$  denotes the capacitor used to couple the  $i$ th and  $j$ th transmon qubits with its nearest-neighbor qubits.  $\phi_j$  refers to node flux expressed in units of reduced flux quantum  $\phi_0 = 1/(2e)$ . The symbol  $\langle i, j \rangle$  indicates that the summation runs over all pairs of the nearest-neighbor sites. With the canonical coordinate  $\hat{\phi}_j$ , the canonical momentum  $\hat{q}_j = \partial L / \partial \hat{\phi}_j$ , i.e.,

$$\hat{q}_j = C_j \hat{\phi}_j + \sum_{j\langle i \rangle} C_j (\hat{\phi}_j - \hat{\phi}_{j\langle i \rangle}) \quad (2)$$

where  $j\langle i \rangle$  is the summation of the nearest-neighbor sites around the  $j$ th site. Considering the experimental condition that  $C_j \gg \{C_{(j-1)j}, C_{j(j+1)}\}$ , we have  $\hat{\phi}_j \approx \hat{q}_j / C_j$ . By applying the Legendre transformation, we obtain the corresponding Hamiltonian

$$\hat{H} = \hat{H}_0 + \hat{H}_{II}, \quad (3)$$

where

$$\hat{H}_0 = \sum_j \left( \frac{\hat{q}_j^2}{2\tilde{C}_j} + \frac{\hat{\phi}_j^2}{2L_j^J} - \frac{E_j^{J0}}{24\hat{\phi}_0^4} \hat{\phi}_j^4 \right), \quad (4)$$

$$\hat{H}_{II} = \sum_{\langle i, j \rangle} \frac{C_{ij}}{C_i C_j} \hat{q}_i \hat{q}_j, \quad (5)$$

with  $1/\tilde{C}_j = (C_j - C_{(j-1)j} - C_{j(j+1)})/C_j^2$  and  $1/L_j^J = E_j^{J0}/\phi_0^2$ .

By introducing bosonic annihilation and creation operators

$$\hat{a}_j = \sqrt{\frac{\tilde{C}_j \omega_j^0}{2}} \hat{\phi}_j + i \sqrt{\frac{1}{2\tilde{C}_j \omega_j^0}} \hat{q}_j, \quad (6)$$

$$\hat{a}_j^\dagger = \sqrt{\frac{\tilde{C}_j \omega_j^0}{2}} \hat{\phi}_j - i \sqrt{\frac{1}{2\tilde{C}_j \omega_j^0}} \hat{q}_j, \quad (7)$$

where  $[\hat{a}_j, \hat{a}_{j'}^\dagger] = \delta_{j, j'}$  and  $\omega_j^0 = \sqrt{8E_j^C E_j^{J0}}$  with  $E_j^C = e^2/(2\tilde{C}_j)$ , and after applying a rotating-wave approximation, the Hamiltonian (3) is quantized as

$$\hat{H}_0 = \sum_j \omega_j^0 \hat{a}_j^\dagger \hat{a}_j + \frac{1}{2} V_j \hat{n}_j (\hat{n}_j - 1), \quad (8)$$

$$\hat{H}_{II} = \sum_j g_j^0 \hat{a}_{(j-1)}^\dagger \hat{a}_j + \text{H.c.}, \quad (9)$$

where H.c. is the Hermitian conjugate,  $\hat{n}_j = \hat{a}_j^\dagger \hat{a}_j$  is the particle number operator, and

$$V_j = -E_j^C, \quad (10)$$

$$g_j^0 = \frac{C_{(j-1)j} \sqrt{\omega_{(j-1)}^0 \omega_j^0}}{2\sqrt{C_{(j-1)j} C_j}}. \quad (11)$$

In Eqs. (8) and (9),  $V_j$  denotes the anharmonicity of each qubit,  $g_j^0$  is the coupling strength between the  $j$ th and  $(j-1)$ th qubits. Since the requirement of  $E_j^C \ll E_j^{J0}$  for transmon qubits[52], we choose  $E_j^{J0}/E_j^C = 50$ ,  $\{C_{(j-1)j}, C_{j(j+1)}\} \approx 0.5$  fF, and  $C_j \approx 100$  fF. Based on these parameters, we obtain  $V_j/(2\pi) \approx 200$  MHz and  $g_j^0/(2\pi) \approx 10$  MHz[53]. This results in a condition that  $V_j \gg g_j^0$ . In such case, the qubit exhibits strong anharmonicity, allowing for only one boson to be excited per transmon qubit. This results in  $V_j \hat{n}_j (\hat{n}_j - 1)/2 \equiv 0$ , and  $\hat{a}_j^\dagger |0\rangle_j = |1\rangle_j$ ,  $\hat{a}_j^\dagger |1\rangle_j = 0$ ,  $\hat{a}_j |0\rangle_j = 0$ , and  $\hat{a}_j |1\rangle_j = |0\rangle_j$ . As a result, the Hamiltonian (3) becomes

$$\hat{H} = \sum_j \omega_j^0 \hat{a}_j^\dagger \hat{a}_j + \sum_j \left( g_j \hat{a}_{(j-1)}^\dagger \hat{a}_j + \text{H.c.} \right). \quad (12)$$

The commutation relation can be reformulated as follows,

$$[\hat{a}_j, \hat{a}_{j'}^\dagger] = (1 - 2\hat{n}_j) \delta_{j, j'}. \quad (13)$$

To achieve tunable coupling strength, an ac microwave driving is applied to each transmon qubit, which can be implemented experimentally via the flux-bias line line[16]. As illustrated in Fig. 1, we incorporate a Josephson junction into a superconducting quantum interference device (SQUID). Since the two Josephson junctions in SQUID possess equal energy, the effective energy can be expressed as  $E_j^J = 2E_j^{J0}$ . As a result of the external magnetic flux  $\Phi_j(t)$ , a phase difference  $\Phi_j(t)/\phi_0$  arises between the two Josephson junctions, leading to a modification in the potential energy of each qubit,

$$\begin{aligned} & E_j^{J0} \left[ \cos \left( \frac{\phi_j}{\phi_0} + \frac{\Phi_j(t)}{2\phi_0} \right) + \cos \left( \frac{\phi_j}{\phi_0} - \frac{\Phi_j(t)}{2\phi_0} \right) \right] \\ &= E_j^J(t) \cos \left( \frac{\phi_j}{\phi_0} \right), \end{aligned} \quad (14)$$

where  $E_j^J(t) = E_j^J \cos[\Phi_j(t)/2\phi_0]$ . The frequency of the  $j$ th qubit becomes  $\omega_j(t) = \omega_j^0 \sqrt{\cos[\Phi_j(t)/2\phi_0]}$ . Here we take the external magnetic flux as,

$$\Phi_j(t) = \alpha_j \cos(u_j^0 t + \phi_j^0), \quad (15)$$

where  $\alpha_j \ll \omega_j^0$ ,  $u_j^0$ , and  $\phi_j^0$  are amplitude, frequency, and phase of the external magnetic flux respectively. Next we conduct Taylor expansion of the frequency  $\omega_j(t)$  at  $\Phi_j(t) = 0$ ,

$$\omega_j(t) \approx \omega_j^0 + \varepsilon_j \sin(u_j t + \phi_j), \quad (16)$$

where  $\varepsilon_j = \omega_j^0 \alpha_j^2 / 4\phi_0^2$ ,  $u_j = 2u_j^0$ , and  $\phi_j = 2\phi_j^0 + 3\pi/2$ . In experiments[16],  $u_j$  is of the order  $\sim 100$  MHz, which is far larger than  $g_j^0$ . Then an unitary operator  $\hat{U} = \hat{U}_A \times \hat{U}_B$  is introduced to transform the Hamiltonian (12) with the frequency  $\omega_j(t)$ , where,

$$\begin{aligned} \hat{U}_A &= \exp \left[ -i \sum_{j=1}^N \omega_j^0 \hat{n}_j t \right] \\ \hat{U}_B &= \exp \left[ i \sum_{j=1}^N f_j \cos(u_j t + \phi_j) \right], \end{aligned} \quad (17)$$

with  $f_j = \varepsilon_j / u_j$  and  $N$  is the number of the qubits. The transformed Hamiltonian can be obtained,

$$\begin{aligned} \hat{H}_t &= \hat{U}^\dagger \hat{H} \hat{U} + i \frac{d\hat{U}}{dt} \hat{U} \\ &= \sum_{j=1}^{N-1} g_j^0 \left\{ e^{-i\Delta_j t} \exp[-if_j \cos(u_j t + \phi_j)] \right. \\ &\quad \left. \exp[if_{j+1} \cos(u_{j+1} t + \phi_{j+1})] \hat{a}_j^\dagger \hat{a}_{j+1} + \text{H.c.} \right\}, \end{aligned} \quad (18)$$

where  $\Delta_j = \omega_{j+1}^0 - \omega_j^0$ . We choose  $\Delta_j = u_{j+1}(-u_j)$  for odd (even)  $j$ . Next we utilize the Jacobi-Anger identity,  $\exp[if_j \cos(u_j t + \phi_j)] = \sum_{m=-\infty}^{\infty} i^m J_m(f_j) \exp[im(u_j t + \phi_j)]$ , and apply the rotating-wave approximation to the Hamiltonian in Eq. (18). Here  $J_m(f_j)$  represents the  $m$ th Bessel function of the first kind. By neglecting the oscillating terms and setting  $\phi_j = -\pi(0)$  for odd (even)  $j$ , we can derive,

$$\hat{H}_{eff} = \sum_{j=1}^{N-1} g_j \left( \hat{a}_j^\dagger \hat{a}_{j+1} + \text{H.c.} \right), \quad (19)$$

where

$$g_j = g_j^0 J_0(f_j) J_1(f_{j+1}) \quad (20)$$

As is evident, the coupling strength  $g_j$  can be tuned independently. For obtaining the SSH model with controllable off-diagonal quasi-periodic modulations, we take  $g_j = g[1 + \lambda + \delta \cos(2\pi\beta j)]$  for odd  $j$  and  $g_j = g[1 - \lambda + \delta \cos(2\pi\beta j)]$  for even  $j$ . For constituting the quasi-periodic disorder, we take  $\beta = (\sqrt{5} - 1)/2$ .  $\lambda$  and  $\delta$  indicate the dimerization and quasi-periodic disorder strengths respectively. In this paper we set  $g = 1$  as the unit of the energy. In the following discussion, we denote the creation (annihilation) operator of the qubit with odd and even  $j$  as  $\hat{a}_i^\dagger$  ( $\hat{a}_i$ ) and  $\hat{b}_i^\dagger$  ( $\hat{b}_i$ ) respectively, where  $i$  is the unit cell index in the case of  $\delta = 0$ . Here we consider the single excitation throughout our work.

### III. PHASE DIAGRAM AND QUANTUM STATE TRANSFER

#### A. Phase diagram

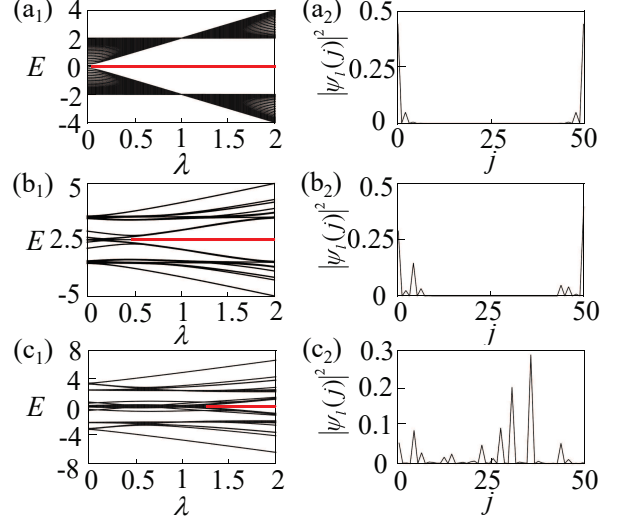


FIG. 2: Energy bands and wave functions of the  $N/2$ th and  $(N/2 + 1)$ th  $[l = N/2, (N/2 + 1)]$  eigenstates for the Hamiltonian in Eq. (19) with open boundary condition. (a<sub>1</sub>)-(c<sub>1</sub>) Energy bands as functions of  $\lambda$  with (a<sub>1</sub>)  $\delta = 0$ , (b<sub>1</sub>)  $\delta = 1$ , and (c<sub>1</sub>)  $\delta = 2$ . (a<sub>2</sub>)-(c<sub>2</sub>) Wave functions with (a<sub>2</sub>)  $\delta = 0$  and  $\lambda = 0.5$ , (b<sub>2</sub>)  $\delta = 1$  and  $\lambda = 0.5$  and (c<sub>2</sub>)  $\delta = 2$  and  $\lambda = 0.5$ .

In this section we focus on the phase diagram resulting from the interplay between quasi-periodic disorder and dimerization strengths. We employ 50 transmon qubits in this section.

When disorder is absent in the generalized SSH model (19), it is reduced to the SSH model. Its energy bands are shown in Fig. 2(a), indicating the presence of degenerate zero-energy modes that persist within the middle of the energy gap, with a value of  $\lambda > 0$ . The corresponding wave functions exhibit exponential localization at the boundaries of the system, as shown in Fig. 2(e). Subsequently, we activate the disorder and present the variation of these energy bands in Figs. 2(b) and (c), demonstrating that as  $\delta$  increases, the energy gap near zero-energy vanishes within the small  $\lambda$  region. Figures 2 (e)-(g) demonstrate the transition of edge states into bulk of the system as  $\delta$  increases. These results demonstrate that strong disorder can only destroy topological states in the case of small  $\lambda$ . This implies that the competition between dimerization strength  $\lambda$  and quasi-periodic disorder strength  $\delta$  can induce a transition from topologically trivial to nontrivial phases. In the following, we will explain these results analytically.

With  $\delta = 0$ , we can ansatz the edge states as  $|\Psi\rangle_{E=0} = \sum_i (\rho_1^i w_1 \hat{a}_i^\dagger \pm \rho_2^i w_2 \hat{b}_i^\dagger) |G\rangle$ , where  $|G\rangle$  is the vacuum state.

According to the Schrödinger equation,  $\hat{H}|\Psi\rangle_{E=0} = 0$ , ie,

$$(g_1\rho_2^i + g_2\rho_2^{i-1})w_2\hat{a}_i^\dagger|G\rangle + (g_2\rho_1^{i+1} + g_1\rho_1^i)w_1\hat{b}_i^\dagger|G\rangle = 0, \quad (21)$$

the edge states can be obtained as

$$|\Psi\rangle_{E=0} = \sum_i \left[ \left( -\frac{g_1}{g_2} \right)^i w_1\hat{a}_i^\dagger \pm \left( -\frac{g_2}{g_1} \right)^i w_2\hat{b}_i^\dagger \right] |G\rangle. \quad (22)$$

These results demonstrate that the state is localized in proximity to the leftmost ( $i = 1$ )  $a$ -type site and rightmost ( $i = N/2$ )  $b$ -type site.

Next, we introduce disorder and observe the changes in  $\rho_1$  and  $\rho_2$ ,

$$\rho_1 = -\frac{1 - \lambda + \delta \cos [2\pi\beta (2i - 1)]}{1 + \lambda + \delta \cos [2\pi\beta (2i)]}, \quad (23)$$

$$\rho_2 = -\frac{1 + \lambda + \delta \cos [2\pi\beta (2i)]}{1 - \lambda + \delta \cos [2\pi\beta (2i - 1)]}, \quad (24)$$

which depend on the qubits' indexes. Equations (23) and (24) indicates the presence of non-zero  $\delta$  prevents  $\rho_1$  and  $\rho_2$  from always being larger or smaller than 1. This implies that the behavior of topological edge states is influenced by  $\delta$ . Then for characterizing distinct topological phases in the case of  $\delta \neq 0$ , we compute the topological invariant. Since the Hamiltonian (19) possesses chiral, time-reversal and particle-hole symmetries, it belongs to class BDI of the Altland-Zirnbauer classification. The topological properties of the system can be characterized by the winding number, which can be easily calculated in momentum space for translationally invariant systems. However, in the presence of non-zero disorder strength, translational symmetry is broken and thus the computation of winding number must be performed in real space using a local quantity[54, 55],

$$\nu = \frac{1}{2} \text{Tr}'(\hat{P}\hat{\Gamma}\hat{X}\hat{P}), \quad (25)$$

where  $\text{Tr}'$  indicate the trace over the single unit cell in the middle of the qubits chain.  $\hat{P} = \hat{P}_+ - \hat{P}_-$  with  $\hat{P}_+$  ( $\hat{P}_-$ ) is the projection operator of the eigenstates with positive (negative) eigenenergies.  $\hat{\Gamma} = \sum_{i=1}^N (\hat{\Gamma}_{a_i}^e - \hat{\Gamma}_{b_i}^e)$  where  $\hat{\Gamma}_{di}^e = |e\rangle_{di}\langle e|$  with  $|e\rangle_{di}$  ( $d = a, b$ ) indicates the state with exciting  $d$ -type qubit at the  $i$ th unit cell.  $\hat{X}$  is the unit-cell position operator. We numerically calculate the winding number in Fig. 3(a). In region III ( $\delta > 1 + \lambda$ ),  $\nu = 0$ , indicating that the system is topologically trivial. In regions I and II ( $\delta < 1 + \lambda$ ),  $\nu = 1$ , indicating that the system is topologically nontrivial. This finding accurately demonstrates that the coexistence of strong disorder and weak dimerization strength can result in the annihilation of topological states.

On the other hand, localization always emerges in a quasi-periodic system. We can capture the localization property of the  $n$ th eigenstate  $|\Psi_n\rangle = \sum_j \psi_n(j) |e\rangle_j$  ( $\psi_n(j)$  is the wave function) in our system by the inverse participation ratio(IPR), which is defined as  $\text{IPR}_n = \sum_j |\psi_n(j)|^4$ . For an extended (a fully localized) state,  $\text{IPR}_n \approx (2N)^{-1}$  ( $\text{IPR}_n \approx 1$ ). For a

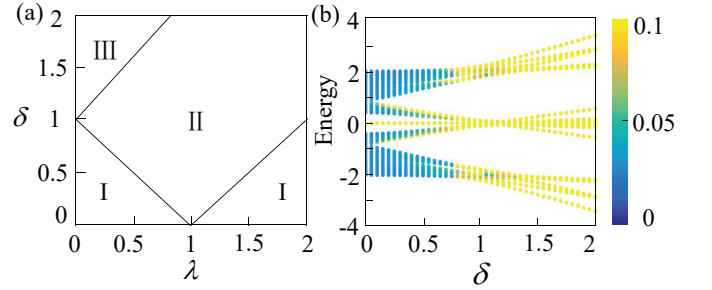


FIG. 3: (a) Phase diagram in the  $\lambda$ - $\delta$  plane. I is extended topologically nontrivial phase with winding number  $\nu = 1$ . II is the coexisting topological critical localization phase with winding number  $\nu = 1$ . III is the critical localization phase with winding number  $\nu = 0$ . (b) Energy bands denoted by the values of  $\text{IPR}_n$  as a function of  $\delta$  with  $\lambda = 0.5$ .

critically localized state,  $\text{IPR}_n \approx (2N)^{-\theta}$ , where  $\theta \in (0, 1)$  depends on the multifractal nature of the wave function. We present the phase diagram in Fig. 3(a) and find our system exhibits localization transition boundaries, where the values of  $\text{IPR}_n$  shift from zero in region I ( $\delta < 1 - \lambda \cup \delta < \lambda - 1$ ) to finite values between 0 and 1 in regions II and III ( $\delta > 1 - \lambda \cap \delta > \lambda - 1$ ). This result suggests that the localization properties are also influenced by the strength of dimerization.

In conclusion, the competition between  $\delta$  and  $\lambda$  induces four different quantum phases which are extended topologically nontrivial [region I in Fig. 3(a)], coexisting topological and critical localization [region II in Fig. 3(a)], and critical localization [region III in Fig. 3(a)] phases. In addition, the energy bands with open boundary condition marked by the values of  $\text{IPR}_n$  are shown in Fig. 3(b), which indicates there are no mobility edges except few edge states.

## B. Quantum state transfer

In this section, we demonstrate the transfer of quantum states both with and without quasi-periodic disorder.

Firstly, considering  $\delta = 0$ , the edge states are presented in Eq.(22). When the number of qubits is even, the edge states will localize at both boundaries of the system. Therefore, regardless of how  $\lambda$  changes, the quantum state localized at leftmost boundary cannot transfer to the rightmost. While in the case of odd qubits, both boundaries are composed of  $a$ -type qubits which result in the localization of edge states at the left- and rightmost boundaries with  $\lambda > 0$  and  $\lambda < 0$ , respectively. This implies the quantum state transfer can occur when  $\lambda$  changes from negative to positive values. To achieve this change, we set  $\lambda = \cos(\gamma)$  with  $\gamma \in [0, \pi]$ . In order to verify this quantum state transfer, the periodic parameter  $\gamma$  should be a function of time  $t$ . Here we choose  $\gamma = \Omega t$  with  $\Omega$  as the rate of change and the initial state is chosen as the leftmost edge state, which can be written as  $|L\rangle = (egg\dots g)$ . We illustrate the temporal evolution of the qubits' excitations in Fig.4(a). This result indicates that the quantum state is trans-

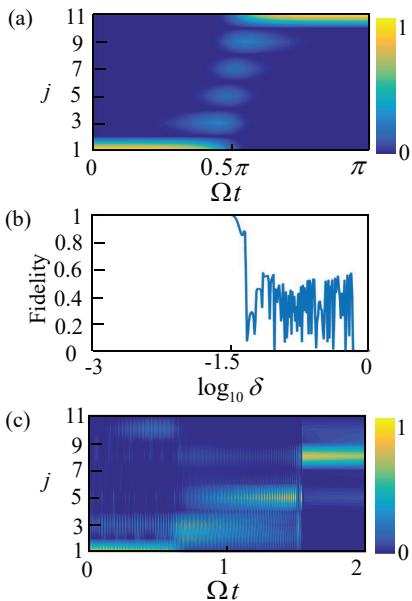


FIG. 4: (a) Time evolution of qubits' excitations with  $\delta = 0$  and  $L = 11$ . (b) The fidelity of the state transfer between  $|L\rangle$  and  $|R\rangle$ . (c) Time evolution of qubits' excited states with  $\lambda = 0.5$  and  $L = 10$

ferred from the leftmost boundary to the rightmost boundary of the system through bulk with  $\gamma$  varying from 0 to  $2\pi$ . Subsequently, we introduce quasi-periodic disorder  $\delta$  and present the fidelity of this quantum state transfer  $F = \langle R | \psi_f \rangle$  in Fig. 4(b).  $|R\rangle = (gg..ge)$  is the rightmost edge state.  $|\psi_f\rangle$  is the final state. When  $\delta$  is sufficiently small, the quantum state transfer persists. While as  $\delta$  increases beyond a certain threshold, the transfer becomes unfeasible.

We then observe the quantum state transfer by varying the quasi-periodic disorder strength  $\delta$ . Similarly to the aforementioned discussion, here we set  $\delta = \Omega t$  and choose  $|L\rangle$  as the initial state. The corresponding temporal evolutions of the qubits' excitations are illustrated in Fig. 4(c). We find the qubits' excitations localize at the leftmost boundary when  $\Omega t$  is smaller than approximately 0.5, which can be attributed to the system being in a topological extended phase as depicted in Fig. 3(a). As  $\Omega t$  varies from 0.5 to 1.5, these excitations depart from the leftmost boundary and diffuse throughout the bulk of the system. In this case, the system is in coexisting topological and critical localization phase [Fig. 3(a)]. Therefore this diffusion arises due to competition between topology and localization. In the region where  $\Omega t > 1.5$ , the qubits' excitations are localized at one or some bulk states of the system due to critical localization phase with topologically trivial properties [Fig. 3(a)]. These results suggest that the quantum state can transfer from a boundary state to certain states within the bulk, which is induced by the interplay between topology and localization.

#### IV. POSSIBLE EXPERIMENTAL OBSERVATION

In this section, we propose an experimental scheme for detecting the aforementioned phases. Furthermore, it is worth noting that the quantum state transfer can be observed directly. In superconducting circuits, the winding number (25)

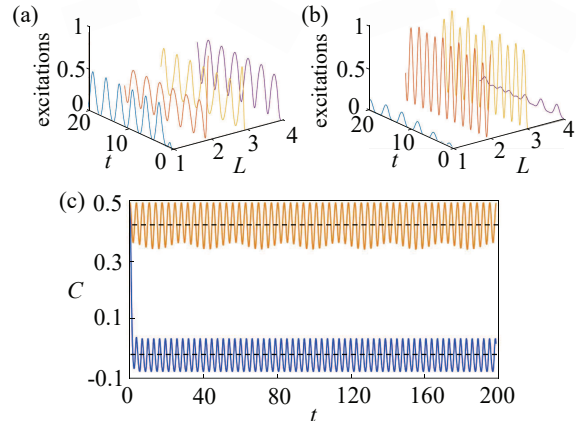


FIG. 5: Time evolution of all qubits' excited states in two dimensional representation with (a)  $\delta = 2$  and (b)  $\delta = 0.2$ . (c) Time evolution of chiral displacement with  $\delta = 2$  and  $\delta = 0.2$  denoted by blue and orange curves, respectively. In all figures  $\lambda = 0.5$

can be dynamically detected through the mean chiral displacement (MCD)  $\bar{C}$  [55–57] with  $\bar{C} = \nu/2$ . The MCD is defined as,

$$\bar{C} = \frac{1}{T} \int_0^T C dt, \quad (26)$$

with  $C = \langle \psi(t) | \hat{\Gamma} \hat{X} | \psi(t) \rangle$ . Here  $|\psi(t)\rangle = e^{-i\hat{H}t} |\psi(0)\rangle$  is the state of the system at time  $t$ .  $|\psi(0)\rangle$  is the initial state. Here we utilize four qubits to detect the MCD. Firstly we prepare an initial state  $|\psi(0)\rangle = |gegg\rangle$ , which excite one of the middle qubits to a excited state and leave the others in ground states. The time evolution of this excitation can be measured directly, which is shown in Fig. 5(a) and (b). We can see, in the topological trivial phase, this excitation can propagate to the boundaries of the qubit chain [Fig. 5(a)], whereas in the topologically nontrivial phase, it is confined within the bulk [Fig. 5(b)]. Subsequently, the time evolution of the CD can be derived, which as depicted in Fig. 5(c). The blue and orange curves denote topological trivial and nontrivial phases respectively. The CD exhibits oscillations around -0.01 and 0.42 in topological trivial and nontrivial phases, respectively, indicating distinct winding numbers of -0.02 and 0.84. This finding is in close proximity to the ideal values.

To identify the critical localization, the detection of  $\text{IPR}_n$  is necessary. The  $\text{IPR}_n$  can be obtained from the eigenstates of Hamiltonian (19). Since each qubit can be represented as a point on the Bloch sphere, the  $j$ th qubit can be denoted by  $|\psi_j\rangle = \cos(\theta_j) |0\rangle_j + e^{i\chi_j} \sin(\theta_j/2) |1\rangle_j$ , where  $\theta_j$  ( $\chi_j$ ) is the angle between the qubit  $|\psi_j\rangle$  and the  $z(x)$  axis in the Bloch

sphere. The eigenstates can be described as  $|\psi\rangle_n = \prod_j |\psi_j\rangle$ . To determine the specific values of the angles  $\theta_j^n$  and  $\chi_j^n$  for the  $n$ th eigenstate, it is necessary to numerically calculate the amplitude of the single-qubit excitation  $\lambda_j^n$  for each qubit in the  $n$ th eigenstate. Then angles  $\theta_j^n$  and  $\chi_j^n$  can be obtained as  $2 \arccos(\sqrt{1 - |\lambda_j^n|^2})$  and  $-i \ln[\lambda_j^n / \sin(\theta_j/2)]$  respectively. The  $n$ th eigenstate can be obtained after applying a rotation operator  $\hat{U}_j^n = e^{i\theta_j^n \hat{\sigma}_z + i\chi_j^n \hat{\sigma}_x}$  for each qubit. This rotation operation can be realized by a microwave pulses. Finally the  $\text{IPR}_n$  can be derived directly.

## V. CONCLUSION

In summary, we have proposed a feasible experimental method to realize the one dimensional SSH model with controllable off-diagonal quasi-periodic modulations on superconducting circuits. For realizing independently tunable cou-

pling strengths, we apply an external ac magnetic flux to drive each transmon qubit. Then the generalized SSH model with both dimerization and quasi-periodic can be constructed. Based on this model, extended topologically nontrivial, critical localization, and coexisting topological and critical localization phases transitions are discovered. We use the winding number and IPR to characterize the topological and localization properties respectively. The dynamics of the qubits' excitations are also discussed in this paper, revealing distinct quantum state transfers resulting from the interplay between topology and localization. Furthermore, we propose a method for detecting different quantum phases using current experimental setups. Notably, we introduce the mean chiral displacement (MCD) as a means to probe the winding number. Our results provide a novel avenue for exploring exotic quantum phases and dynamic behaviors arising from the interplay between dimerization and quasi-periodic disorder strengths on superconducting circuits.

- 
- [1] Iulia Buluta, Sahel Ashhab, and Franco Nori. Natural and artificial atoms for quantum computation. *Reports on Progress in Physics*, 74(10):104401, 2011.
  - [2] Ming Gong, Shiyu Wang, Chen Zha, Ming-Cheng Chen, He-Liang Huang, Yulin Wu, Qingling Zhu, Youwei Zhao, Shaowei Li, Shaojun Guo, Qian Haoran, Ye Yangsen, Chen Fusheng, Ying Chong, Yu Jiale, Fan Daojin, Wu Dachao, Su Hong, Deng Hui, Rong Hao, Zhang Kaili, Cao Sirui, Jin Lin, Yu Xu, Lihua Sun, Cheng Guo, Na Li, Futian Liang, M. Bastidas, V., Nemoto Kae, J. Munro, W., Yong-Heng Huo, Chao-Yang Lu, Cheng-Zhi Peng, Xiaobo Zhu, and Jian-Wei Pan. Quantum walks on a programmable two-dimensional 62-qubit superconducting processor. *Science*, 372(6545):948–952, 2021.
  - [3] Tong Liu, Bao-Qing Guo, Chang-Shui Yu, and Wei-Ning Zhang. One-step implementation of a hybrid fredkin gate with quantum memories and single superconducting qubit in circuit qed and its applications. *Optics express*, 26(4):4498–4511, 2018.
  - [4] Göran Wendin. Quantum information processing with superconducting circuits: a review. *Reports on Progress in Physics*, 80(10):106001, 2017.
  - [5] Chui-Ping Yang and Zhen-Fei Zheng. Deterministic generation of greenberger–horne–zeilinger entangled states of cat-state qubits in circuit qed. *Optics Letters*, 43(20):5126–5129, 2018.
  - [6] Alexandre Blais, Steven M Girvin, and William D Oliver. Quantum information processing and quantum optics with circuit quantum electrodynamics. *Nature Physics*, 16(3):247–256, 2020.
  - [7] Iulia M Georgescu, Sahel Ashhab, and Franco Nori. Quantum simulation. *Reviews of Modern Physics*, 86(1):153, 2014.
  - [8] Xueyue Zhang, Eunjong Kim, Daniel K Mark, Soonwon Choi, and Oskar Painter. A superconducting quantum simulator based on a photonic-bandgap metamaterial. *Science*, 379(6629):278–283, 2023.
  - [9] Chong Ying, Bin Cheng, Youwei Zhao, He-Liang Huang, Yuning Zhang, Ming Gong, Yulin Wu, Shiyu Wang, Futian Liang, Jin Lin, Xu Yu, Deng Hui, Rong Hao, Peng Cheng-Zhi, Yung Man-Hong, Zhu Xiaobo, and Jian-Wei Pan. Experimental simulation of larger quantum circuits with fewer superconducting qubits. *Physical review letters*, 130(11):110601, 2023.
  - [10] Da-Wei Wang, Chao Song, Wei Feng, Han Cai, Da Xu, Hui Deng, Hekang Li, Dongning Zheng, Xiaobo Zhu, H Wang, Shi-Yao Zhu, and O Scully. Synthesis of antisymmetric spin exchange interaction and chiral spin clusters in superconducting circuits. *Nature Physics*, 15(4):382–386, 2019.
  - [11] Xinseng Tan, Dan-Wei Zhang, Qiang Liu, Guangming Xue, Hai-Feng Yu, Yan-Qing Zhu, Hui Yan, Shi-Liang Zhu, and Yang Yu. Topological maxwell metal bands in a superconducting qutrit. *Physical review letters*, 120(13):130503, 2018.
  - [12] Xinseng Tan, YX Zhao, Qiang Liu, Guangming Xue, Hai-Feng Yu, ZD Wang, and Yang Yu. Simulation and manipulation of tunable weyl-semimetal bands using superconducting quantum circuits. *Physical review letters*, 122(1):010501, 2019.
  - [13] Zhiguang Yan, Yu-Ran Zhang, Ming Gong, Yulin Wu, Yarui Zheng, Shaowei Li, Can Wang, Futian Liang, Jin Lin, Yu Xu, Cheng Guo, Lihua Sun, Zhi-Cheng Peng, Keyu Xia, Hui Deng, Hao Rong, Q You, J, Franco Nori, Heng Fan, Xiaobo Zhu, and Jian-Wei Pan. Strongly correlated quantum walks with a 12-qubit superconducting processor. *Science*, 364(6442):753–756, 2019.
  - [14] Kuljeet Kaur, Théo S epulcre, Nicolas Roch, Izak Snyman, Serge Florens, and Soumya Bera. Spin-boson quantum phase transition in multilevel superconducting qubits. *Physical Review Letters*, 127(23):237702, 2021.
  - [15] James Dborin, Vinul Wimalaweera, Fergus Barratt, Eric Ostby, Thomas E O'Brien, and Andrew G Green. Simulating ground-state and dynamical quantum phase transitions on a superconducting quantum computer. *Nature Communications*, 13(1):5977, 2022.
  - [16] Xuegang Li, Y Ma, J Han, Tao Chen, Y Xu, W Cai, H Wang, YP Song, Zheng-Yuan Xue, Zhang-qi Yin, and Luyan Sun. Perfect quantum state transfer in a superconducting qubit chain with parametrically tunable couplings. *Physical Review Applied*, 10(5):054009, 2018.
  - [17] Weizhou Cai, Jiaxiu Han, Feng Mei, Yuan Xu, Yuwei Ma, Xuegang Li, Haiyan Wang, YP Song, Zheng-Yuan Xue, Zhang-qi Yin, Suotang Jia, and luyan Sun. Observation of topological

- magnon insulator states in a superconducting circuit. *Physical review letters*, 123(8):080501, 2019.
- [18] M Zahid Hasan and Charles L Kane. Colloquium: topological insulators. *Reviews of modern physics*, 82(4):3045, 2010.
- [19] Xiao-Liang Qi and Shou-Cheng Zhang. Topological insulators and superconductors. *Reviews of Modern Physics*, 83(4):1057, 2011.
- [20] Alexander B Khanikaev, S Hossein Mousavi, Wang-Kong Tse, Mehdi Kargarian, Allan H MacDonald, and Gennady Shvets. Photonic topological insulators. *Nature materials*, 12(3):233–239, 2013.
- [21] Mikael C Rechtsman, Julia M Zeuner, Yonatan Plotnik, Yaakov Lumer, Daniel Podolsky, Felix Dreisow, Stefan Nolte, Mordechai Segev, and Alexander Szameit. Photonic floquet topological insulators. *Nature*, 496(7444):196–200, 2013.
- [22] Joseph Maciejko and Gregory A Fiete. Fractionalized topological insulators. *Nature Physics*, 11(5):385–388, 2015.
- [23] János K Asbóth, László Oroszlány, and András Pályi. A short course on topological insulators. *Lecture notes in physics*, 919:166, 2016.
- [24] Stephan Rachel. Interacting topological insulators: a review. *Reports on Progress in Physics*, 81(11):116501, 2018.
- [25] Frank Schindler, Ashley M Cook, Maia G Vergniory, Zhijun Wang, Stuart SP Parkin, B Andrei Bernevig, and Titus Neupert. Higher-order topological insulators. *Science advances*, 4(6):eaat0346, 2018.
- [26] Yoshinori Tokura, Kenji Yasuda, and Atsushi Tsukazaki. Magnetic topological insulators. *Nature Reviews Physics*, 1(2):126–143, 2019.
- [27] Mark S Rudner and Netanel H Lindner. Band structure engineering and non-equilibrium dynamics in floquet topological insulators. *Nature reviews physics*, 2(5):229–244, 2020.
- [28] Tobias Biesenthal, Lukas J Maczewsky, Zhaoju Yang, Mark Kremer, Mordechai Segev, Alexander Szameit, and Matthias Heinrich. Fractal photonic topological insulators. *Science*, 376(6597):1114–1119, 2022.
- [29] Ying Lei, Xi-Wang Luo, and Shaoliang Zhang. Second-order topological insulator in periodically driven optical lattices. *Optics Express*, 30(13):24048–24061, 2022.
- [30] Jian Li, Rui-Lin Chu, Jainendra K Jain, and Shun-Qing Shen. Topological anderson insulator. *Physical review letters*, 102(13):136806, 2009.
- [31] CW Groth, M Wimmer, AR Akhmerov, J Tworzydło, and CWJ Beenakker. Theory of the topological anderson insulator. *Physical review letters*, 103(19):196805, 2009.
- [32] H-M Guo, G Rosenberg, G Refael, and M Franz. Topological anderson insulator in three dimensions. *Physical review letters*, 105(21):216601, 2010.
- [33] Simon Stützer, Yonatan Plotnik, Yaakov Lumer, Paraj Titum, Netanel H Lindner, Mordechai Segev, Mikael C Rechtsman, and Alexander Szameit. Photonic topological anderson insulators. *Nature*, 560(7719):461–465, 2018.
- [34] Eric J Meier, Fangzhao Alex An, Alexandre Dauphin, Maria Maffei, Pietro Massignan, Taylor L Hughes, and Bryce Gadway. Observation of the topological anderson insulator in disordered atomic wires. *Science*, 362(6417):929–933, 2018.
- [35] Bing Yang, Hongfang Zhang, Qiang Shi, Tong Wu, Yong Ma, Zengtao Lv, Xia Xiao, Ruixin Dong, Xunling Yan, and Xiangdong Zhang. Details of the topological state transition induced by gradually increased disorder in photonic chern insulators. *Optics Express*, 28(21):31487–31498, 2020.
- [36] Weixuan Zhang, Deyuan Zou, Qingsong Pei, Wenjing He, Jiacheng Bao, Houjun Sun, and Xiangdong Zhang. Experimental observation of higher-order topological anderson insulators. *Physical Review Letters*, 126(14):146802, 2021.
- [37] JB Sokoloff. Unusual band structure, wave functions and electrical conductance in crystals with incommensurate periodic potentials. *Physics Reports*, 126(4):189–244, 1985.
- [38] DJ Thouless. Localization by a potential with slowly varying period. *Physical review letters*, 61(18):2141, 1988.
- [39] Pedram Roushan, Charles Neill, J Tangpanitanon, Victor M Bastidas, A Megrant, Rami Barends, Yu Chen, Z Chen, B Chiaro, A Dunsworth, A Fowler, B Foxen, M Giustina, E Jeffrey, J Kelly, E Lucero, J Mutus, M Neeley, C Quintana, D Sank, A Vainsencher, J Wenner, T White, H Neven, G Angelakis, D, and J Martinis. Spectroscopic signatures of localization with interacting photons in superconducting qubits. *Science*, 358(6367):1175–1179, 2017.
- [40] Fangzhao Alex An, Karmela Padavić, Eric J Meier, Suraj Hegde, Sriram Ganeshan, JH Pixley, Smitha Vishveshwara, and Bryce Gadway. Interactions and mobility edges: Observing the generalized aubry-andré model. *Physical review letters*, 126(4):040603, 2021.
- [41] Fan Ye and Xiankai Sun. Hofstadter butterfly and topological edge states in a quasiperiodic photonic crystal cavity array. *Optics Express*, 30(15):26620–26627, 2022.
- [42] Ying Yang and Dawei Cao. Observation of the topological phase transition from the spatial correlation of a biphoton in a one-dimensional topological photonic waveguide array. *Optics Express*, 30(21):37899–37909, 2022.
- [43] W-P Su, JR Schrieffer, and Ao J Heeger. Solitons in polyacetylene. *Physical review letters*, 42(25):1698, 1979.
- [44] DJJ Marchand, G De Filippis, V Cataudella, M Berciu, N Nagaosa, NV Prokof'Ev, AS Mishchenko, and PCE Stamp. Sharp transition for single polarons in the one-dimensional su-schrieffer-heeger model. *Physical review letters*, 105(26):266605, 2010.
- [45] Eric J Meier, Fangzhao Alex An, and Bryce Gadway. Observation of the topological soliton state in the su-schrieffer-heeger model. *Nature communications*, 7(1):13986, 2016.
- [46] Bo Xing, Wei-Ting Chiu, Dario Poletti, Richard T Scalettar, and George Batrouni. Quantum monte carlo simulations of the 2d su-schrieffer-heeger model. *Physical Review Letters*, 126(1):017601, 2021.
- [47] Yiqi Zhang, Boquan Ren, Yongdong Li, and Fangwei Ye. Topological states in the super-ssh model. *Optics Express*, 29(26):42827–42836, 2021.
- [48] Mitchell Kiczynski, SK Gorman, Helen Geng, MB Donnelly, Yousun Chung, Yu He, JG Keizer, and MY Simmons. Engineering topological states in atom-based semiconductor quantum dots. *Nature*, 606(7915):694–699, 2022.
- [49] Amir Youssefi, Shingo Kono, Andrea Bancora, Mahdi Chegnizadeh, Jiahe Pan, Tatiana Vovk, and Tobias J Kippenberg. Topological lattices realized in superconducting circuit optomechanics. *Nature*, 612(7941):666–672, 2022.
- [50] Ziteng Wang, Xiangdong Wang, Zhichan Hu, Domenico Bongiovanni, Dario Jukić, Liqin Tang, Daohong Song, Roberto Morandotti, Zhigang Chen, and Hrvoje Buljan. Sub-symmetry-protected topological states. *Nature Physics*, pages 1–7, 2023.
- [51] Mei-Song Wei, Ming-Jie Liao, Ce Wang, Chengjie Zhu, Yaping Yang, and Jingping Xu. Topological laser with higher-order corner states in the 2-dimensional su-schrieffer-heeger model. *Optics Express*, 31(3):3427–3440, 2023.
- [52] Jens Koch, M Yu Terri, Jay Gambetta, Andrew A Houck, David I Schuster, Johannes Majer, Alexandre Blais, Michel H Devoret, Steven M Girvin, and Robert J Schoelkopf. Charge-insensitive qubit design derived from the cooper pair box. *Physical Review A*, 76(4):042319, 2007.

- [53] Yangsen Ye, Zi-Yong Ge, Yulin Wu, Shiyu Wang, Ming Gong, Yu-Ran Zhang, Qingling Zhu, Rui Yang, Shaowei Li, Futian Liang, Jin Lin, Yu Xu, Cheng Guo, Lihua Sun, Chen Cheng, Nvsen Ma, Yang Meng, Zi, Hui Deng, Hao Rong, Chao-Yang Lu, Cheng-Zhi Peng, Heng Fan, Xiaobo Zhu, and Jian-Wei Pan. Propagation and localization of collective excitations on a 24-qubit superconducting processor. *Physical review letters*, 123(5):050502, 2019.
- [54] Ian Mondragon-Shem, Taylor L Hughes, Juntao Song, and Emil Prodan. Topological criticality in the chiral-symmetric aiii class at strong disorder. *Physical review letters*, 113(4):046802, 2014.
- [55] Eric J Meier, Fangzhao Alex An, Alexandre Dauphin, Maria Maffei, Pietro Massignan, Taylor L Hughes, and Bryce Gadway. Observation of the topological anderson insulator in disordered atomic wires. *Science*, 362(6417):929–933, 2018.
- [56] Eric J Meier, Fangzhao Alex An, and Bryce Gadway. Observation of the topological soliton state in the su–schrieffer–heeger model. *Nature communications*, 7(1):13986, 2016.
- [57] Filippo Cardano, Alessio D’Errico, Alexandre Dauphin, Maria Maffei, Bruno Piccirillo, Corrado de Lisio, Giulio De Filippis, Vittorio Cataudella, Enrico Santamato, Lorenzo Marrucci, Maciej Lewenstein, and Pietro Massignan. Detection of zak phases and topological invariants in a chiral quantum walk of twisted photons. *Nature communications*, 8(1):15516, 2017.



